This is the accepted manuscript made available via CHORUS. The article has been published as:

Omnidirectional domain wall modes protected by fragile topological states

Pegah Azizi, Siddhartha Sarkar, Kai Sun, and Stefano Gonella

Phys. Rev. B **110**, L060102 — Published 20 August 2024

DOI: 10.1103/PhysRevB.110.L060102

Omni-directional domain wall modes protected by fragile states

Pegah Azizi,[1] Siddhartha Sarkar,[2] Kai Sun,[2] and Stefano Gonella[1,*]

[1]*Department of Civil, Environmental, and Geo- Engineering, University of Minnesota, Minneapolis, MN 55455, US*

[2]*Department of Physics, University of Michigan, Ann Arbor, MI 48109, USA*

(Dated: August 8, 2024)

So-called fragile topological states of matter challenge our conventional notion of topology by lacking the robustness typically associated with topological protection, thereby displaying elusive manifestations that are difficult to harness for wave control. In this Letter, we leverage the recent discovery of fragile topological states in special classes of structural kagome lattices to document the availability of domain wall elastic wave modes that are directly traceable to fragile topology and, yet, exhibit remarkably strong signatures that support omni-directionality. We design twisted kagome bi-domains comprising two topologically distinct sublattices - one trivial and the other fragile topological - sharing a common bandgap and meeting at a domain wall. The two phases are achieved via carefully engineered surface cut patterns that modify the band landscape of the underlying lattices in complementary fashions, leading to dichotomous irreps landscapes. Under these circumstances, a domain wall-bound mode emerges within the shared bandgap and displays remarkable stability against domain wall orientation and introduced defects. We corroborate these findings via $\mathbf{k}\cdot\mathbf{p}$ Hamiltonian and Jackiw-Rabbi analysis and validate them experimentally through laser vibrometry tests on a prototype endowed with water jet-induced perforation patterns.

Maxwell lattices [1, 2] have received substantial attention in recent years due to an array of unique mechanical properties, including the ability to localize deformation at floppy edges [3–7] and focus stress at domain walls (DWs), thus eliciting protection against fracture and buckling [8, 9], and tunable multistability [10]. A popular subclass of Maxwell systems, kagome lattices have been extensively studied, especially in the realm of ideal configurations characterized by perfect hinges, for the peculiar properties rooted in their topology and symmetries [11–17]. Many topological properties of Maxwell lattices have been shown to be preserved, albeit diluted, in transitioning from *ideal* to *structural* lattices that can be physically fabricated, where the bonds can carry flexural deformation and the hinges are replaced by internal clamps or by ligaments featuring finite stiffness against rotations [18–23].

Recent studies have put forth the notion of fragile topology [24–35]. Fragile bands qualify as topological in that they do not admit a symmetric, exponentially localized Wannier representation that preserves all the symmetries of the system. However, unlike stable topology, their obstruction to the atomic limit can be eliminated by coupling with fully topologically trivial bands. Additionally, these states generally lack a well defined conventional bulk-edge correspondence [36–40]. A recent investigation by Azizi et al. explored fragile topology in the context of twisted kagome lattices in the so-called self-dual configuration [18]. The term *self-dual*, introduced by Fruchart et al. within their treatment of mechanical duality of twisted kagome lattices [41] refers to the critical point in configuration space that separates families of dual pairs, which feature identical phononic properties [12, 41, 42]. The authors of [18] proved theoretically and demonstrated experimentally the existence of fragile topological states in self-dual kagome lattices in the *structural* configuration featuring ligament-like hinges at the lattice sites. However, while they identified a number of localized modes, for none of them a direct connection to fragile topology or claims of topological protection could be made.

This Letter aims at filling this conceptual gap by deliberately searching for localized modes that are unequivocally linked to, and protected by, the fragile topology. We seek such modes along the DWs of bi-domain lattices obtained by adjoining two structural self-dual twisted kagome (SSTK) sublattices with different topological character - one trivial and the other fragile topological - making sure that the two phases are designed to be spectrally compatible. The proposed approach draws partial inspiration from the behavior of mechanical analogs of the quantum valley-Hall effect (QVHE) [43–47], where domain-bound modes can be generated at the DW of two subdomains characterized by opposite valley topologies bounding a shared bandgap (BG) [48]. A by-product objective of our study is to address a limitation of QVHE analogs, which support DW modes along various orientations [49, 50] except for specific forbidden directions. In contrast, here we put forth a strategy to achieve truly omni-directional DW mode localization capability along any arbitrary direction.

We begin our analysis resuming the SSTK configuration presented in [18], which features fragile topological bands. Recall that the configuration consists of a self-dual kagome in which the triangles are solid patches, taken to be thin to realize plane-stress conditions, connected by finite-thickness ligaments. Our objective is to extract from this baseline geometry two topologically distinct derivative configurations - one trivial and the other topological - that are simultaneously geometrically and

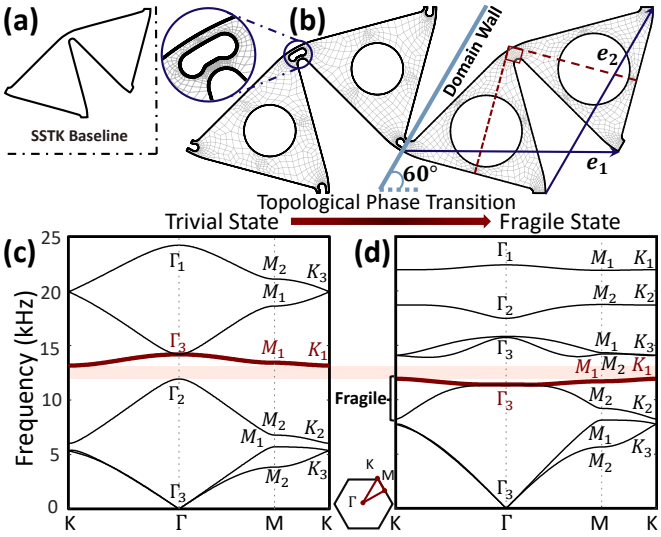


FIG. 1. (a) Unit cell of SSTK baseline configuration. (b) Bi-domain lattice with DW obtained stitching a trivial and a fragile topological SSTK phases. Zoomed-in detail of the bean-shaped hole at the hinge of the trivial phase is presented in the inset. Both configurations feature large holes to modulate inertia and control frequency spectra. (c-d) Band diagrams of the trivial and fragile topological states, respectively. The thick maroon branch denotes the band undergoing inversion, leading to the closing and reopening of the shared BG (shaded in pink) marking the topological phase transition. The irreps at HSPs of the BZ confirm the topological nature of the third and fourth bands in (d).

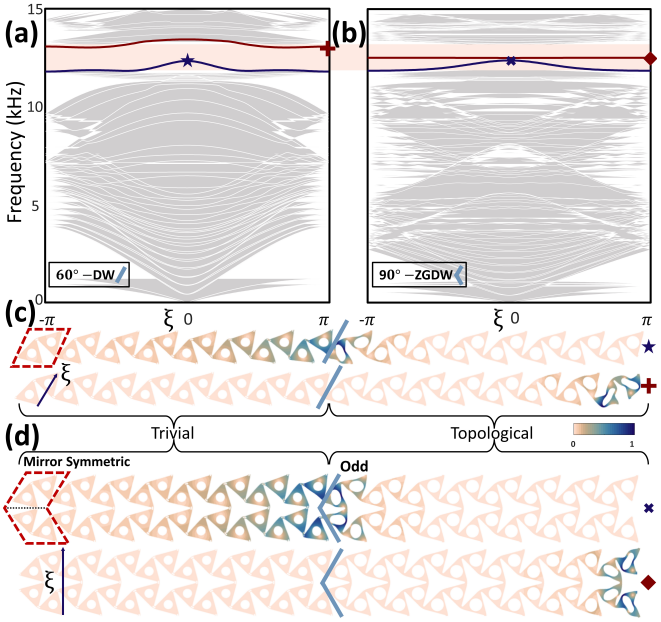


FIG. 2. (a-b) Band diagrams for two differently oriented 16-cell SSTK supercells (with unit cells highlighted) forming (a) 60°−DW and (b) 90°−ZGDW, with branches for the DW mode and edge modes highlighted in blue and maroon, respectively. (c-d) Wave functions (mode shapes) of localized DW and edge states for the 60°−DW and 90°−ZGDW, sampled at $\xi = 0$ and $\xi = \pi$. The left and right sides consist of trivial and topological states, respectively.

spectrally compatible. Geometric compatibility requires that the lattices can be seamlessly stitched to form a DW, which implies that they shall share the same unit cell primitive lattice vectors and C_{3v} point group symmetry. Moreover, in anticipation of the construction of an experimental prototype, we seek configurations that are practically feasible under the constraints of the available fabrication methods. Specifically, we want the lattices to be mono-material, as to be agilely obtainable via subtractive manufacturing (e.g., machining or water-jet cutting) from a slab of homogeneous, low-damping material with uniform and predictable properties, e.g., a metal. We also require that the two lattices deviate from each other only in terms of different patterns of cuts introduced a posteriori as a perturbation of the shared baseline SSTK geometry. This ensures that the thickness of the hinges, which is a critical parameter, is preserved across the DW. Finally, we want the two configurations to be spectrally compatible, i.e., to feature a shared full BG in the mid-frequency region of the spectrum.

The first step of the design process consists of modifying the topological SSTK baseline configuration (Fig. 1(a)) to induce a transition to a trivial configuration, marked by the closing and reopening of the mid-frequency BG. An avenue towards this phase transition is by softening the hinge ligament of the unit cell as explored in [18]. In light of the above-stated mono-material constraint, here we seek an analogous softening effect purely by virtue of geometry. To this end, we introduce isolated cuts or clusters of cuts in the neighborhood of the hinges. After a few design iterations (supplemental material (SM), Sec. 1. [51]), we eventually land on the bean-shaped hole shown in the inset of Fig. 1(b). Notably, this addition results in the desired topological band inversion along with a substantial increase in BG width (SM, Sec. 1. [51]). To ensure spectral compatibility between the new trivial (with hole) and the original topological (hole-less) configurations, we modulate their effective mass densities by endowing the unit cells of both configurations with additional holes and we fine tune their relative diameters until the two BGs have comparable width and align in the desired interval of the spectrum. The resulting geometries are shown in Fig. 1(b) in their stitched configuration, with the trivial phase featuring hinge holes and small density-correcting holes on the left of the DW, and the topological phase featuring intact hinges and large density-correcting holes on the right. The primitive lattice vectors are denoted as $\mathbf{e}_1$ and $\mathbf{e}_2$, with $\mathbf{e}_2$ aligned parallel to the DW, forming a 60° angle with the horizontal. The corresponding band diagrams are shown in Figs. 1(c-d), where we can observe the above-mentioned band inversion at the Γ point, whereby the fourth band (highlighted in maroon)

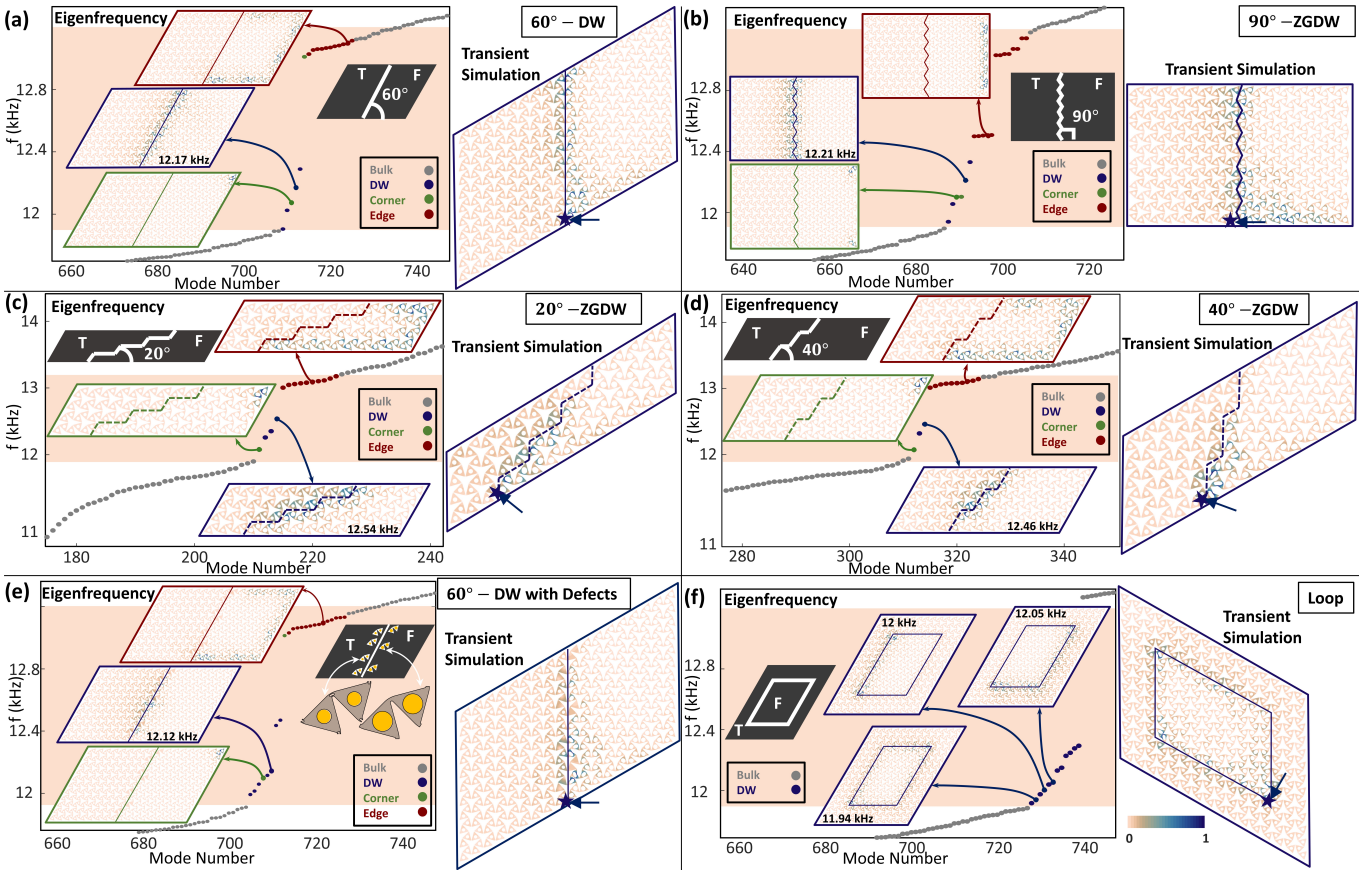


FIG. 3. (a-f) Dynamical response for six scenarios: (a) 60°−DW, (b) 90°−ZGDW, (c) 20°−ZGDW, (d) 40°−ZGDW, (e) 60°−DW with randomly located defects, and (f) internal loop. For each case, the left panel contains eigenfrequencies in the frequency interval of the shared BG, color-coded to distinguish bulk modes and different types of localized modes, including DW (with the corresponding frequency indicated), corner, and edge states, with three sample eigenfields shown in the insets. The right panel depicts snapshots of propagating wavefields (from full-scale transient simulations) induced by a narrow-band burst force excitation, polarized perpendicularly to the DW. In all cases, the wave is unequivocally localized along the DW.

appears above and below the shared BG, respectively. Additionally, we report irreducible representations (irreps) calculated at the high symmetry points (HSPs) of the Brillouin zone (BZ) following the procedure and notation given in the Bilbao crystallography server [52–56] based on the recently developed method of topological quantum chemistry, which classifies all topological states that are protected by spatial symmetries [57, 58]. The irreps, which encapsulate the symmetry properties of the eigenmodes at the HSPs, provide a recipe to qualify the topology of isolated bands. The 2-dimensional (2D) irrep Γ_3 and 1D irrep Γ_2 undergo band inversion from Fig. 1(c) to 1(d) resulting in bands $3-4$ having HSP irreps $\Gamma_3-M_1\oplus M_2-K_1\oplus K_2$ in Fig. 1(d), which implies these two bands are indeed fragile topological, protected by C_3 symmetry [18, 29].

Having established a DW across which a topological phase transition occurs, we proceed to ask whether such DW can be the site of strongly localized modes and whether such modes enjoy any protection that is attributable to the fragile topology. Here, we consider two distinct versions of the bi-domain lattice that can be realized by stitching trivial and fragile phases, one featuring a 60°−DW and the other 90°−zigzag DW (ZGDW). For each, we perform supercell analysis using a dedicated supercell. Specifically, the first supercell (Fig. 2(c)) is obtained from the tessellation of a single SSTK unit cell and intercepts the 60°−DW already discussed in Fig. 1. The other (Fig. 2(d)) consists of the tessellation of a mirror symmetric macrocell encompassing two unit cells, and results in a 90°−ZGDW globally perpendicular to the supercell itself and parallel to the direction of tessellation. The corresponding supercell band diagrams are shown in Figs. 2(a-b), respectively. In both configurations, we identify two relatively flat modes in the BG, which we recognize, from the mode shapes depicted in Figs. 2(c-d), as a DW mode and an edge mode, color-coded in blue and maroon, respectively. The DW mode presents a few peculiarities. First, the availability of DW modes for both 60°−DW and 90°−ZGDW (as well as potentially along any other arbitrary direction, as demonstrated later in the Letter) represents an increase in versatility compared

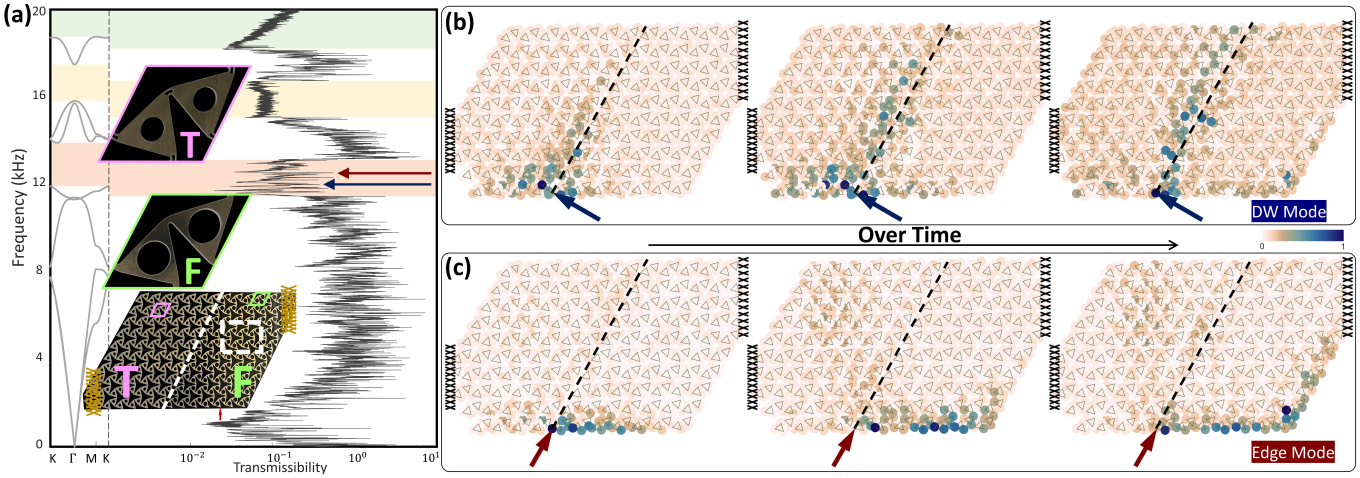


FIG. 4. (a) Laser vibrometry-acquired experimental transmissibility curve with highlighted attenuation regions reasonably matching the BG frequencies of the fragile phase spectrum plotted on the left. Insets provide details of the trivial (T) and fragile (F) unit cells of the water jet-cut specimen. White dashed box denotes a region where response is sampled. Blue and maroon arrows mark the excitation frequencies for the DW and edge modes activation, respectively. (b-c) Snapshots of the measured wavefields induced by 30-cycle burst with carrier frequencies corresponding to the DW and edge modes. Force polarization is indicated by the arrows. Color bar indicates velocity amplitude normalized by the highest value in each frame.

to QVHE, where DW modes are not achievable for angles of 90° (and equivalently 30° and 150°) (SM, Sec. 2. [51]). Here, the emergence of DW modes for any angle can be understood from the isotropic nature of the Γ point in a C_3 symmetric system. Moreover, most conventional topologically protected DW branches span the BG with quasi-constant finite slopes, denoting modes that propagate at finite velocities for any carrier frequency in the BG [44, 45]. Here, in contrast, the relatively flat band results in the ability of the lattice to localize the signal in space with pronounced persistence over a frequency subinterval of the BG, while maintaining the response overall gapped. As for the edge modes, it is worth noting that they appear only in the fragile phase, where they display a high decay rate.

The emergence of the DW modes resulting from the topological phase transition marked by the band inversion between the Γ_2 and Γ_3 irreps, can be analytically confirmed using Jackiw-Rebbi (JR) analysis [59]. In SM, Sec. 2. [51], starting from a $\mathbf{k}\cdot\mathbf{p}$ Hamiltonian [60] near the Γ point of the BZ and considering only the bands with Γ_2 and Γ_3 irreps, we theoretically prove that DW modes must emerge between the trivial and fragile phases for any DW direction. Furthermore, we prove that the DW mode shapes obtained from the supercell analysis, shown in Figs. 2(c-d), are indeed caused by the topological phase transition between the trivial and fragile states by comparing them against those obtained from the JR analysis. It is worthwhile mentioning that, since the 90°−ZGDW is mirror symmetric, a DW mode at this interface would have to be even or odd under the mirror reflection. It can be seen from Fig. 2(d) that the DW mode has indeed odd parity under the mirror- a feature captured by JR analysis. On the other hand, the 60°−DW breaks the mirror symmetry, hence the DW mode does not have a definite parity, also predicted by the JR analysis.

Next, we evaluate eigenfrequencies and mode shapes for six finite bi-domain configurations depicted in Fig. 3, including 60°−DW (Fig. 3(a)), 90°−ZGDW (Fig. 3(b)), 20°−ZGDW (Fig. 3(c)), 40°−ZGDW (Fig. 3(d)), 60°−DW with defects (Fig. 3(e)), and loop (Fig. 3(f)). In the configuration of Fig. 3(e), we randomly select seven unit cells close to the DW and we fill their central holes with inclusions, choosing a density ratio $\rho_{inc} = 0.8\rho_{bulk}$ to perturb the lattice order. In each of the cases in Figs. 3(a-e), we report localized states in the BG frequency range: we recognize DW, corner, and edge modes, and we highlight a few randomly selected ones for each type by showing the corresponding eigenfunctions. Notably, in Figs. 3(a-e), edge and corner modes localize exclusively along the edges of the fragile phase, consistent with the findings from supercell analysis. Finally, in the case of Fig. 3(f), we construct a closed DW loop to confine a parallelogram of fragile phase within a larger domain of the trivial phase and we perform a similar inference of the localized modes.

Subsequently, we provide additional evidence of DW emergence in the considered scenarios via full-scale transient simulations. Snapshots of computed propagating wavefields are displayed in the right part of each panel of Figs. 3(a-f) under a point-force excitation, polarized perpendicular to the DW, prescribed at the bottom tip of the DW in the form of a 17-cycle narrow-band tone burst, with carrier frequency set at ∼12.2 kHz. Notably, in all cases, the wavefields exhibit pronounced localization along the DW, regardless of the DW orientation and

the presence of defects.

We proceed to validate our theoretical findings through laser vibrometry experiments performed on a physical prototype (for detailed information regarding the fabrication, vibrometer specifications, and experimental setup refer to SM, Sec. 3. [51]). The specimen, along with zoomed-in details of the fragile and trivial unit cells, are displayed in the insets of Fig. 4(a). Our initial objective is to experimentally determine the BG frequencies. To accomplish this, we prescribe a broadband pseudorandom vertical excitation at a bottom edge point of the fragile phase (marked by a red arrow), we measure the in-plane vertical velocity at scan points inside a sampling region located away from the DW and the edges (dashed box in the inset of Fig. 4(a)), and we normalize the average velocity values with those recorded at the excitation point to construct a transmissibility curve versus frequency, as presented in Fig. 4(a) (See SM, Sec. 4. [51] for analogous curves obtained via full-scale steady-state simulation). Notably, the transmissibility reveals three distinct regions of attenuation, highlighted in lighter shades, which align well, within the expected deviations between model and experiments, with the BGs derived from Bloch analysis. The region shaded in pink marks the mid-frequency BG of interest, within which we carry out two separate transient tests to empirically document the emergence of DW and edge modes. To this end, we excite the bottom tip of the DW with bursts with carrier frequencies marked by the blue and maroon arrows in Fig. 4(a). We note that the frequency discrepancies between model and experiments prevent us from being able to know precisely the frequency of the localized modes a priori. Similarly, the transmissibility plot does not carry a sufficient spectral signature of them that can be leveraged. As a result, the identification of the carriers requires a heuristic approach in which we probe the frequency interval expected to be of interest based on analogy with simulations by conducting a series of tests with varying carriers until we detect the emergence of the desired modes. Eventually, we identify 12 kHz and 12.5 kHz as the two frequencies of interest for the DW and edge modes, respectively. Specifically, if we apply a 30-cycle burst with a frequency of $\sim$12 kHz, polarized perpendicular to the DW direction, we generate a wave that propagates along the DW, three snapshots of which are depicted in Fig.4(b). Similarly, Fig. 4(c) presents three snapshots of a wave induced by an excitation with a carrier frequency of $\sim$12.5 kHz, polarized parallel to the DW, which features localization along the edge (of the fragile phase only, consistent with the eigenmode prediction). In summary, in all cases we record strong localization that persists even deep into the propagation process, before reflections from the opposite boundary begin to interfere with the incident wave to form a standing pattern.

P.A. acknowledges the support of the UMN CSE Graduate Fellowship. S.G. acknowledges support from the National Science Foundation (grant CMMI-2027000). S.S. and K.S. acknowledge the support from the Office of Naval Research (grant MURI N00014-20-1-2479).

* sgonella@umn.edu

[1] J. Clerk Maxwell, "L. on the calculation of the equilibrium and stiffness of frames," The London, Edinburgh, and Dublin Philosophical Magazine and Journal of Science **27**, 294–299 (1864).

[2] C.R. Calladine, "Buckminster fuller's "tensegrity" structures and clerk maxwell's rules for the construction of stiff frames," International Journal of Solids and Structures **14**, 161–172 (1978).

[3] Xiaoming Mao and Tom C. Lubensky, "Maxwell lattices and topological mechanics," Annual Review of Condensed Matter Physics **9**, 413–433 (2018).

[4] Xiaoming Mao and T. C. Lubensky, "Coherent potential approximation of random nearly isostatic kagome lattice," Phys. Rev. E **83**, 011111 (2011).

[5] C. L. Kane and T. C. Lubensky, "Topological boundary modes in isostatic lattices," Nature Physics **10**, 39–45 (2014).

[6] T C Lubensky, C L Kane, Xiaoming Mao, A Souslov, and Kai Sun, "Phonons and elasticity in critically coordinated lattices," Reports on Progress in Physics **78**, 073901 (2015).

[7] D. Zeb Rocklin, Shangnan Zhou, Kai Sun, and Xiaoming Mao, "Transformable topological mechanical metamaterials," Nature Communications **8** (2017), 10.1038/ncomms14201.

[8] Leyou Zhang and Xiaoming Mao, "Fracturing of topological maxwell lattices," New Journal of Physics **20**, 063034 (2018).

[9] Jayson Paulose, Anne S. Meussen, and Vincenzo Vitelli, "Selective buckling via states of self-stress in topological metamaterials," Proceedings of the National Academy of Sciences **112**, 7639–7644 (2015).

[10] Haning Xiu, Harry Liu, Andrea Poli, Guangchao Wan, Kai Sun, Ellen M. Arruda, Xiaoming Mao, and Zi Chen, "Topological transformability and reprogrammability of multistable mechanical metamaterials," Proceedings of the National Academy of Sciences **119**, e2211725119 (2022).

[11] Kai Sun, Anton Souslov, Xiaoming Mao, and T. C. Lubensky, "Surface phonons, elastic response, and conformal invariance in twisted kagome lattices," Proceedings of the National Academy of Sciences **109**, 12369–12374 (2012).

[12] Hrishikesh Danawe, Heqiu Li, Hasan Al Ba'ba'a, and Serife Tol, "Existence of corner modes in elastic twisted kagome lattices," Phys. Rev. B **104**, L241107 (2021).

[13] Hussein Nassar, Hui Chen, and Guoliang Huang, "Microtwist elasticity: A continuum approach to zero modes and topological polarization in kagome lattices," Journal of the Mechanics and Physics of Solids **144**, 104107 (2020).

[14] H. Chen, H. Nassar, A. N. Norris, G. K. Hu, and G. L. Huang, "Elastic quantum spin hall effect in kagome lattices," Phys. Rev. B **98**, 094302 (2018).

[15] E. Riva, D. E. Quadrelli, G. Cazzulani, and F. Braghin,

"Tunable in-plane topologically protected edge waves in continuum kagome lattices," Journal of Applied Physics **124**, 164903 (2018).

[16] Marshall Schaeffer and Massimo Ruzzene, "Wave propagation in reconfigurable magneto-elastic kagome lattice structures," Journal of Applied Physics **117**, 194903 (2015).

[17] Katia Bertoldi, Vincenzo Vitelli, Johan Christensen, and Martin van Hecke, "Flexible mechanical metamaterials," Nature Reviews Materials **2**, 17066 (2017).

[18] Pegah Azizi, Siddhartha Sarkar, Kai Sun, and Stefano Gonella, "Dynamics of self-dual kagome metamaterials and the emergence of fragile topology," Phys. Rev. Lett. **130**, 156101 (2023).

[19] Mohammad Charara, Kai Sun, Xiaoming Mao, and Stefano Gonella, "Topological flexural modes in polarized bilayer lattices," Phys. Rev. Applied **16**, 064011 (2021).

[20] Caleb Widstrand, Chen Hu, Xiaoming Mao, Joseph Labuz, and Stefano Gonella, "Stress focusing and damage protection in topological maxwell metamaterials," International Journal of Solids and Structures **274**, 112268 (2023).

[21] Hui Chen, Shaoyun Wang, Xiaopeng Li, and Guoliang Huang, "Two-dimensional microtwist modeling of topological polarization in hinged kagome lattices and its experimental validation," International Journal of Solids and Structures **254-255**, 111891 (2022).

[22] Jihong Ma, Di Zhou, Kai Sun, Xiaoming Mao, and Stefano Gonella, "Edge modes and asymmetric wave transport in topological lattices: Experimental characterization at finite frequencies," Phys. Rev. Lett. **121**, 094301 (2018).

[23] Zi-Dong Zhang, Ming-Hui Lu, and Yan-Feng Chen, "Twist-angle-induced boundary-obstructed topological insulator on elastic kagome metamaterials," Phys. Rev. Appl. **20**, 054002 (2023).

[24] Hoi Chun Po, Haruki Watanabe, and Ashvin Vishwanath, "Fragile topology and wannier obstructions," Physical review letters **121**, 126402 (2018).

[25] Barry Bradlyn, Zhijun Wang, Jennifer Cano, and B. Andrei Bernevig, "Disconnected elementary band representations, fragile topology, and wilson loops as topological indices: An example on the triangular lattice," Phys. Rev. B **99**, 045140 (2019).

[26] Junyeong Ahn, Sungjoon Park, and Bohm-Jung Yang, "Failure of nielsen-ninomiya theorem and fragile topology in two-dimensional systems with space-time inversion symmetry: Application to twisted bilayer graphene at magic angle," Phys. Rev. X **9**, 021013 (2019).

[27] Adrien Bouhon, Annica M. Black-Schaffer, and Robert-Jan Slager, "Wilson loop approach to fragile topology of split elementary band representations and topological crystalline insulators with time-reversal symmetry," Phys. Rev. B **100**, 195135 (2019).

[28] Benjamin J Wieder and B Andrei Bernevig, "The axion insulator as a pump of fragile topology," arXiv preprint arXiv:1810.02373 (2018), arXiv:1810.02373.

[29] Zhi-Da Song, Luis Elcoro, and B. Andrei Bernevig, "Twisted bulk-boundary correspondence of fragile topology," Science **367**, 794–797 (2020).

[30] Valerio Peri, Zhi-Da Song, Marc Serra-Garcia, Pascal Engeler, Raquel Queiroz, Xueqin Huang, Weiyin Deng, Zhengyou Liu, B. Andrei Bernevig, and Sebastian D. Huber, "Experimental characterization of fragile topology in an acoustic metamaterial," Science **367**, 797–800 (2020).

[31] Benjamin J Wieder, Zhijun Wang, Jennifer Cano, Xi Dai, Leslie M Schoop, Barry Bradlyn, and B Andrei Bernevig, "Strong and fragile topological dirac semimetals with higher-order fermi arcs," Nature communications **11**, 1–13 (2020).

[32] Biao Lian, Fang Xie, and B. Andrei Bernevig, "Landau level of fragile topology," Phys. Rev. B **102**, 041402 (2020).

[33] Adrien Bouhon, Tomá š Bzdušek, and Robert-Jan Slager, "Geometric approach to fragile topology beyond symmetry indicators," Phys. Rev. B **102**, 115135 (2020).

[34] María Blanco de Paz, Maia G. Vergniory, Dario Bercioux, Aitzol García-Etxarri, and Barry Bradlyn, "Engineering fragile topology in photonic crystals: Topological quantum chemistry of light," Phys. Rev. Res. **1**, 032005 (2019).

[35] Valerio Peri, Zhi-Da Song, B. Andrei Bernevig, and Sebastian D. Huber, "Fragile topology and flat-band superconductivity in the strong-coupling regime," Phys. Rev. Lett. **126**, 027002 (2021).

[36] Yuanfeng Xu, M. G. Vergniory, Da-Shuai Ma, Juan L. Mañes, Zhi-Da Song, B. Andrei Bernevig, Nicolas Regnault, and Luis Elcoro, "Catalogue of topological phonon materials," (2022).

[37] F. Nur Ünal, Adrien Bouhon, and Robert-Jan Slager, "Topological euler class as a dynamical observable in optical lattices," Phys. Rev. Lett. **125**, 053601 (2020).

[38] Bo Peng, Adrien Bouhon, Bartomeu Monserrat, and Robert-Jan Slager, "Phonons as a platform for non-abelian braiding and its manifestation in layered silicates," Nature Communications **13** (2022), 10.1038/s41467-022-28046-9.

[39] Sander Kooi, Guido van Miert, and Carmine Ortix, "The bulk-corner correspondence of time-reversal symmetric insulators," npj Quantum Materials **6** (2021), 10.1038/s41535-020-00300-7.

[40] A. Alexandradinata, J. Höller, Chong Wang, Hengbin Cheng, and Ling Lu, "Crystallographic splitting theorem for band representations and fragile topological photonic crystals," Phys. Rev. B **102**, 115117 (2020).

[41] Michel Fruchart, Yujie Zhou, and Vincenzo Vitelli, "Dualities and non-abelian mechanics," Nature **577**, 636–640 (2020).

[42] Hrishikesh Danawe, Heqiu Li, Kai Sun, and Serife Tol, "Finite-frequency topological maxwell modes in mechanical self-dual kagome lattices," Phys. Rev. Lett. **129**, 204302 (2022).

[43] E. C. Marino, Leandro O. Nascimento, Van Sérgio Alves, and C. Morais Smith, "Interaction induced quantum valley hall effect in graphene," Phys. Rev. X **5**, 011040 (2015).

[44] Raj Kumar Pal and Massimo Ruzzene, "Edge waves in plates with resonators: an elastic analogue of the quantum valley hall effect," New Journal of Physics **19**, 025001 (2017).

[45] Jihong Ma, Kai Sun, and Stefano Gonella, "Valley hall in-plane edge states as building blocks for elastodynamic logic circuits," Phys. Rev. Appl. **12**, 044015 (2019).

[46] Ting-Wei Liu and Fabio Semperlotti, "Experimental evidence of robust acoustic valley hall edge states in a nonresonant topological elastic waveguide," Phys. Rev. Appl.

11, 014040 (2019).
[47] Kai Qian, David J. Apigo, Camelia Prodan, Yafis Barlas, and Emil Prodan, "Topology of the valley-chern effect," Phys. Rev. B **98**, 155138 (2018).
[48] Hui Pan, Xin Li, Fan Zhang, and Shengyuan A. Yang, "Perfect valley filter in a topological domain wall," Phys. Rev. B **92**, 041404 (2015).
[49] Yi Chen, Xiaoning Liu, and Gengkai Hu, "Topological phase transition in mechanical honeycomb lattice," Journal of the Mechanics and Physics of Solids **122**, 54–68 (2019).
[50] Xiaoxiao Wu, Yan Meng, Jingxuan Tian, Yingzhou Huang, Hong Xiang, Dezhuan Han, and Weijia Wen, "Direct observation of valley-polarized topological edge states in designer surface plasmon crystals," Nature Communications **8** (2017), 10.1038/s41467-017-01515-2.
[51] "See supplemental material at ... for details, including the following: Design process of deriving two topologically distinct lattices and topological phonon band inversion, $\mathbf{k}\cdot\mathbf{p}$ Hamiltonian and Jackiw-Rebbi analysis of the DW mode, Experimental set up, and Full-scale steady-state simulation transmissibility curve,".
[52] Mois I Aroyo, Juan Manuel Perez-Mato, Danel Orobengoa, EMRE Tasci, Gemma de la Flor, and Asel Kirov, "Crystallography online: Bilbao crystallographic server," Bulg. Chem. Commun **43**, 183–197 (2011).
[53] Mois Ilia Aroyo, Juan Manuel Perez-Mato, Cesar Capillas, Eli Kroumova, Svetoslav Ivantchev, Gotzon Madariaga, Asen Kirov, and Hans Wondratschek, "Bilbao crystallographic server: I. databases and crystallographic computing programs," Zeitschrift für Kristallographie-Crystalline Materials **221**, 15–27 (2006).
[54] Mois I Aroyo, Asen Kirov, Cesar Capillas, JM Perez-Mato, and Hans Wondratschek, "Bilbao crystallographic server. ii. representations of crystallographic point groups and space groups," Acta Crystallographica Section A: Foundations of Crystallography **62**, 115–128 (2006).
[55] M. G. Vergniory, L. Elcoro, Zhijun Wang, Jennifer Cano, C. Felser, M. I. Aroyo, B. Andrei Bernevig, and Barry Bradlyn, "Graph theory data for topological quantum chemistry," Phys. Rev. E **96**, 023310 (2017).
[56] Luis Elcoro, Barry Bradlyn, Zhijun Wang, Maia G. Vergniory, Jennifer Cano, Claudia Felser, B. Andrei Bernevig, Danel Orobengoa, Gemma de la Flor, and Mois I. Aroyo, "Double crystallographic groups and their representations on the Bilbao Crystallographic Server," Journal of Applied Crystallography **50**, 1457–1477 (2017).
[57] Barry Bradlyn, Luis Elcoro, Jennifer Cano, Maia G Vergniory, Zhijun Wang, Claudia Felser, Mois I Aroyo, and B Andrei Bernevig, "Topological quantum chemistry," Nature **547**, 298–305 (2017).
[58] Jennifer Cano, Barry Bradlyn, Zhijun Wang, L. Elcoro, M. G. Vergniory, C. Felser, M. I. Aroyo, and B. Andrei Bernevig, "Building blocks of topological quantum chemistry: Elementary band representations," Phys. Rev. B **97**, 035139 (2018).
[59] R. Jackiw and C. Rebbi, "Solitons with fermion number," Phys. Rev. D **13**, 3398–3409 (1976).
[60] M.S. Dresselhaus, G. Dresselhaus, and A. Jorio, Group Theory: Application to the Physics of Condensed Matter (Springer Berlin Heidelberg, 2007).